buildings

MDPI

Article

An Optimization Study on Continuous Steel Box Girder Bridge Components

Ang Wang [1,*], Ruiyuan Gao [1], Qingfeng Chen [2], Weizhun Jin [2,*], Pengfei Fang [3] and Di Wu [4]

[1] Civil Engineering and Construction Center, Huanghe Science and Technology University, Zhengzhou 450061, China; gry@hhstu.edu.cn
[2] College of Civil Engineering, Henan University of Engineering, Zhengzhou 451191, China; chenqingfeng@haue.edu.cn
[3] College of Civil Engineering, Henan University of Technology, Zhengzhou 450001, China; fangpf2018@163.com
[4] College of Construction Engineering, Jilin University, Changchun 130012, China; dwu21@mails.jlu.edu.cn
* Correspondence: wangang@hhstu.edu.cn (A.W.); j_weizhun@163.com (W.J.)

Abstract: The steel box girder bridge is a structure composed of mutually vertical stiffening ribs (longitudinal ribs and transverse ribs) that carry the loads of vehicles. Since the external loads are usually complex and variable, the rational design of the bridge components is a topic that deserves more attention. The purpose of this study is to explore the optimal range of some of the component design parameters, expecting to reduce costs while ensuring the stress-carrying capacity. A finite element model (FEM) based on ABAQUS was built and the results were verified by laboratory experiments. The varied thicknesses of the bridge deck, diaphragm, and U-rib were explored based on the validated FEM. The simulation results fit well with the experimental results, which proved that the FEM was quite reliable. The stress analysis results demonstrated an optimal range of 18–20 mm for bridge deck thickness, 14–16 mm for diaphragm thickness, and 8–10 mm for U-rib thickness. The present study holds significant reference value for the design and optimization of multiple steel box girder bridge components, which could further provide a theoretical foundation for related research in this field.

Keywords: continuous steel box girder bridge; component thickness; optimized design; finite element model

Academic Editors: Hsuan-Teh Hu and Tinghua Yi

Received: 29 October 2024
Revised: 24 December 2024
Accepted: 29 December 2024
Published: 3 January 2025

Citation: Wang, A.; Gao, R.; Chen, Q.; Jin, W.; Fang, P.; Wu, D. An Optimization Study on Continuous Steel Box Girder Bridge Components. *Buildings* **2025**, *15*, 124. https://doi.org/10.3390/buildings15010124

1. Introduction

The tensile, compressive, and shear properties of steel box girder bridges prove to be significantly superior when compared to other types of bridges [1–4]. However, due to various factors such as structural characteristics, stress characteristics, and processing technologies, numerous challenging problems remain unsolved [5–7]. Enhancing and optimizing the design of steel box girder bridges to ensure their durability and cost-effectiveness has been an issue that deserves more attention.

An in-depth understanding of the mechanical properties of steel box girder bridges can provide an important reference for the design, construction, and structural health monitoring and assessment of these bridges [8–13]. Tsakopoulos et al. [14] conducted multiple full-scale model tests to study the fatigue performance of the welded joint between the U-rib and diaphragms. Luo et al. [15] investigated the stress distribution and magnitude of an orthotropic steel bridge deck in a cable-stayed bridge through model calculations and experiments. This study analyzed the impact of structural parameters such as longitudinal rib form, U-rib height, and panel thickness, providing valuable insights into the stress

pattern. Zhao et al. [16] investigated the distribution of residual stress in hybrid steel U-rib stiffened plates using the blind hole method. The results indicated that the strain release factor has a significant impact on the calculated residual stress. Further exploration into the mechanical behavior of orthotropic monolithic steel bridge deck systems revealed that increasing the flange thickness of U-ribs could influence their bending and shear capacities [17]. An experimental and numerical analysis of welding residual stresses in U-rib stiffened plates revealed the substantial impacts of welding parameters on stress distributions, which indicated that poor welding quality can exacerbate stress concentrations, potentially leading to premature failure [18]. Lin et al. [19] performed a stress performance analysis on steel bridge decks and identified significant bending stress and subsequent cracking in components due to out-of-plane bending moments caused by the relatively thin bridge deck and U-ribs. Li et al. [20] applied modern branch theory methods to determine the mechanical characteristics of orthotropic rectangular plates in multiple buckling states.

The study of mechanical mechanisms ultimately serves the optimal design of steel box girder bridges. Wei et al. [21] proposed a novel bi-directional U-ribbed stiffening plate (BUSP)—a concrete composite bridge deck—to address the cracking issues in orthotropic steel bridge decks and concrete in negative moment regions. Fu et al. [22] proposed that increasing the bridge deck thickness was effective in slowing down the rate of crack expansion and improving durability. Zhang et al. [23] clarified that increasing the size of the soldering foot can effectively reduce the cracking of the bridge decks at the corresponding locations. Saunders et al. [24] proposed a new diaphragm opening form called a slit cut-out and proved its advantages. Jiang et al. [25] proposed utilizing an iron-based shape memory alloy (Fe-SMA) to enhance the diaphragm notch to improve the structural fatigue performance and effectively extend the structural service life. Duan et al. [26] analyzed the progress of the optimization of steel bridge panels from three perspectives: the selection of strong and ductile combined layers, the interfacial force transfer mechanism and the damage accumulation mechanism, and the design methodology and engineering applications. Jiang et al. [27] proposed the use of carbon fiber-reinforced polymer to improve the fatigue resistance of U-ribs. Freitas et al. [28] suggested that a new steel plate could be added to the surface of the original bridge deck to increase the overall bending stiffness of the structure. Chen et al. [29] proposed the introduction of UHPC rigid paving, which could improve the overall stiffness of steel bridge decks. Da et al. [30] pointed out that optimizing the formal configuration of U-ribs could avoid stress concentrations. Similarly, De Corte [31] suggested that a larger U-rib notch radius can significantly reduce the stress concentration at the corresponding location. Currently, the main focus of the research on optimizable components is shown in Table 1. It can be seen that previous studies have typically focused on the optimization of a single component. Since a steel box girder bridge is a complex structure, a synchronized study for multiple components is obviously more valuable. In this study, the optimal range of bridge deck thickness, diaphragm thickness, and U-rib thickness were explored, which could provide a more comprehensive reference for the design of steel box girder bridges.

While many previous studies have focused on the optimization of a single component, this study simultaneously considered multiple key components including the bridge decks, U-ribs, and diaphragms, which can provide a more comprehensive solution for the optimal design of bridges. In this study, an FEM based on ABAQUS was built to complete the numerical analysis and the results were verified by experiments. The varied thicknesses of the bridge deck, diaphragm, and U-rib were explored based on the validated FEM. This study can provide an important reference for the optimized design of multiple key components of steel bridges, which could play an important role in bridge construction.

Table 1. The literature review of optimizable components.

Author	Year	Components
Wei et al. [21]	2023	Bridge deck
Fu et al. [22]	2017	Bridge deck
Zhang et al. [23]	2020	Soldering foot
Saunders et al. [24]	2021	Diaphragm
Jiang et al. [25]	2024	Diaphragm
Duan et al. [26]	2024	Bridge deck
Jiang et al. [27]	2023	U-ribs
Freitas et al. [28]	2017	Bridge deck
Chen et al. [29]	2019	Bridge deck
Da et al. [30]	2022	U-ribs
De Corte [31]	2009	U-ribs

2. Materials and Methods

The purpose of this study is to optimize the design of multiple key components of a steel box girder bridge, which was built in Harbin, Heilongjiang Province, China. A finite element simulation was the main method used to improve efficiency and reduce costs. In addition, experiments are also necessary to verify the accuracy of the FEM. This study could be divided into 3 main steps: (1) Considering practicality, the computational cost, and the validation cost, build an FEM to simulate a real bridge. (2) Validate the established FEM based on a laboratory experiment. (3) Explore a comprehensive optimization scheme based on the validated FEM. The specific flowchart of this study is shown in Figure 1.

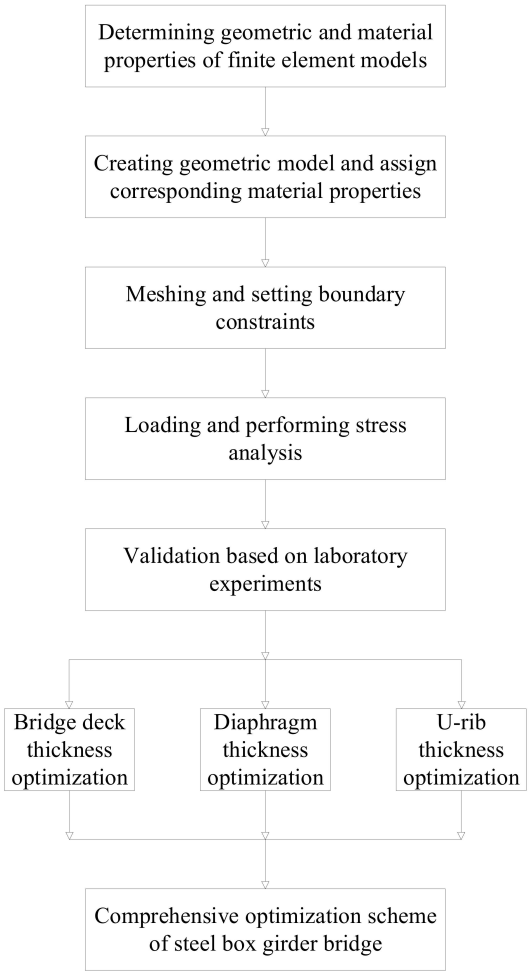

Figure 1. The flowchart of this study.

2.1. Finite-Element Simulations

(1) Geometry and material properties.

In this study, the ABAQUS 2023 software was used to implement an FEM. Compared to an actual bridge, the scaling of the model used in this paper is 10:1. The geometric properties are shown in Figure 2.

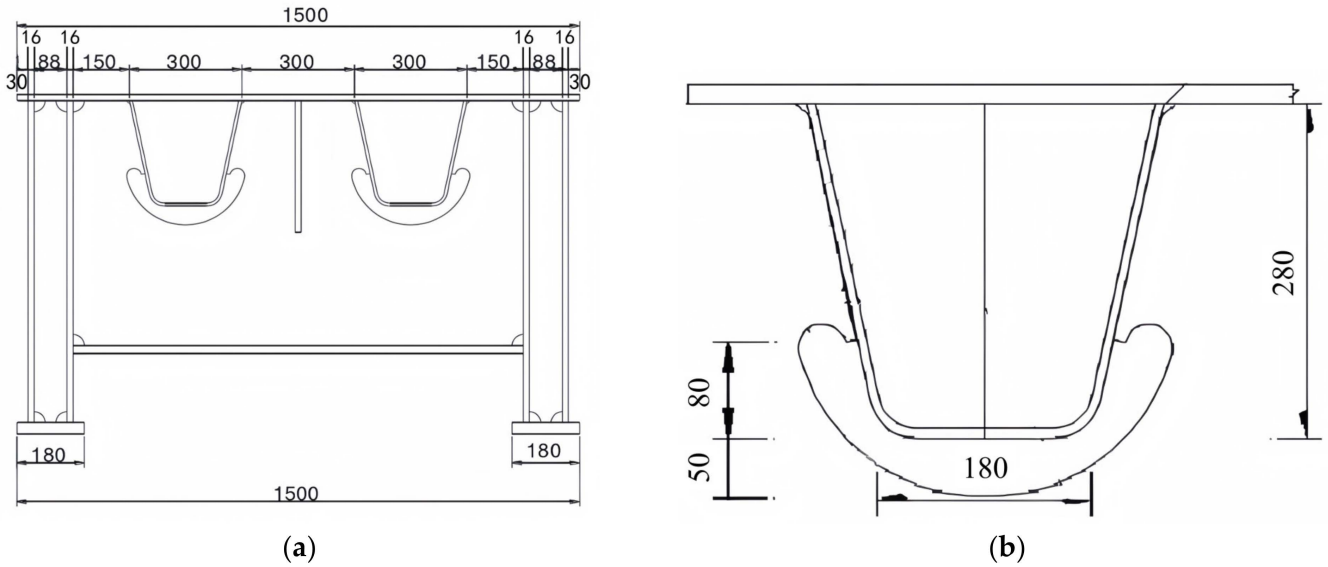

Figure 2. Dimensions of the model (mm): (**a**) Schematic diagram of cross-section; (**b**) Schematic diagram of local dimensions of U-rib and diaphragm.

All the materials of the components were made of Q345 ordinary carbon steel, which was usually regarded as a type of elastic–plastic material. According to a previous study [32], the parameters of Q345 ordinary carbon steel are shown in Table 2.

Table 2. Parameters of Q345 ordinary carbon steel at the elastic–plastic stage.

Modulus of Elasticity (MPa)	Yield Strength (MPa)	Poisson's Ratio	True Stress 1 (MPa)	True Plastic Strain 1	True Stress 2 (MPa)	True Plastic Strain 2
210,000	345	0.3	345.5663	0	537.7247	0.071099

(2) Unit type and mesh size.

The unit type of all the components is C3D8R, which is less prone to shear self-locking and will rarely be affected by a twisting of the meshes. In general, the smaller the mesh size, the higher the accuracy of the results [33]. On the other hand, a smaller mesh size also means more time consumption. For the steel bridge decks and the steel boxes, the mesh size is determined to be 20 mm. For the areas with complex external loads including the U-ribs and curved notches, the mesh seed size is determined to be 10 mm (Figure 3). Finally, a total of 16,485 elements were applied for the simulation.

(3) Boundary and loading conditions

The way in which the boundary conditions are applied is important in a finite simulation analysis [34,35]. Specifically, the constraints on the left side of the model were set as U1 = U2 = UR2 = UR3 = 0, while the right side of the model was set to the full fixed constraint U1 = U2 = U3 = UR1 = UR2 = UR3 = 0. According to the "Regulations on the Management of Over-limit Transportation Vehicles Traveling on Highways", the heaviest standard truck has a gross weight of about 48 tons, which is why we have determined the load to be 480 KN. Three kinds of loading conditions were considered (Figure 4).

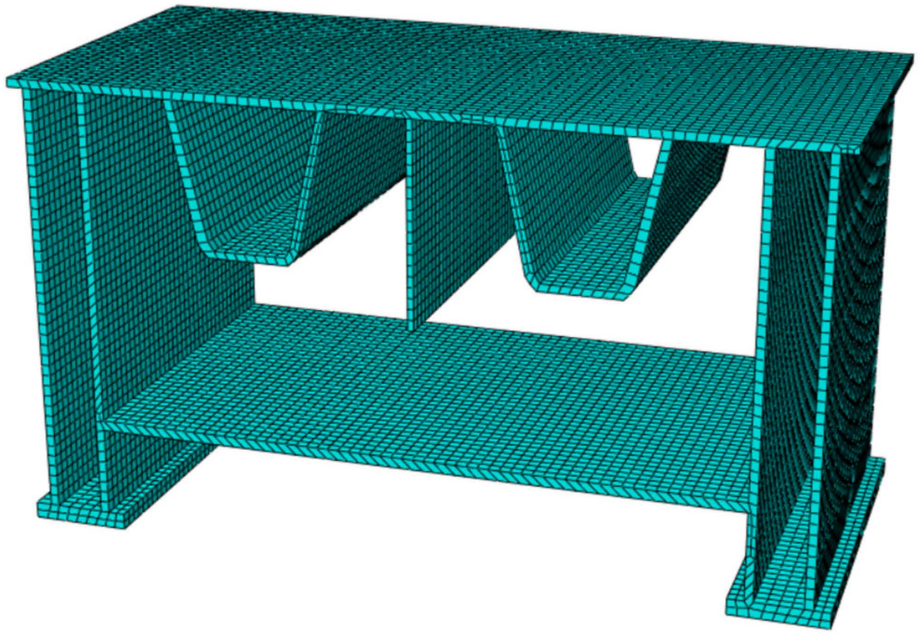

Figure 3. Schematic diagram of FEM meshing.

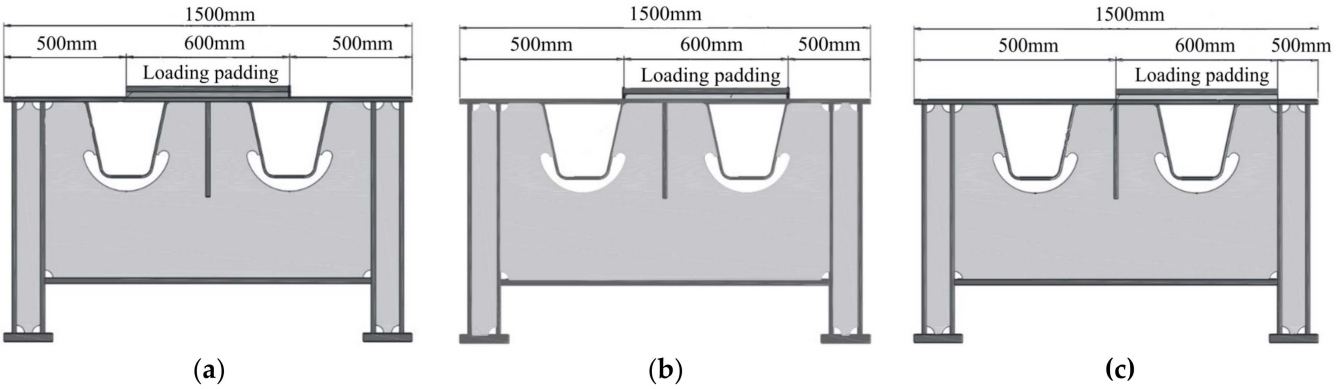

Figure 4. Schematic of loading locations: (**a**) loading condition 1; (**b**) loading condition 2; and (**c**) loading condition 3.

2.2. Laboratory Experiments Validation

An experiment was carried out to verify the rationality of the FEM (Figure 5). The dimensions and properties of the model are consistent with the numerical model. The test was conducted by a PLS-500 electro-hydraulic servo fatigue testing machine, which was manufactured by Docer Testing Machine Co. in Jinan, Shandong Province, China. The arrangement of the strain gauges is shown in Figure 6. The processes are as follows: (1) Preload a load of 50 kN and repeat the loading three times to check for the smooth connection of each part. (2) Once the strain gauge is fully applied and the wires are connected to the data collection instrument, collect and record the initial data. (3) Apply the loads of 80 N, 180 N, 280 N, 380 N, and 480 N, sequentially, and collect and record the experimental data during the stabilization of each loading stage. (4) Change the loading location and repeat the test procedure. It should be noted that the room temperature should be 20–35 °C and the relative humidity should be less than 80%.

Figure 5. Schematic diagram of the experimental model.

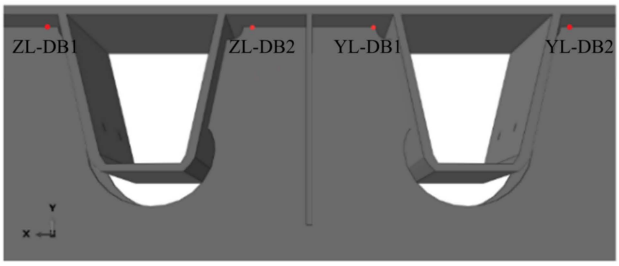

(**a**)

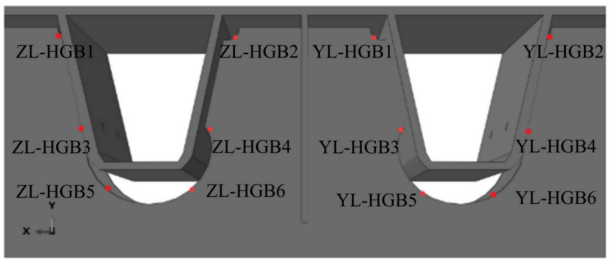

(**b**)

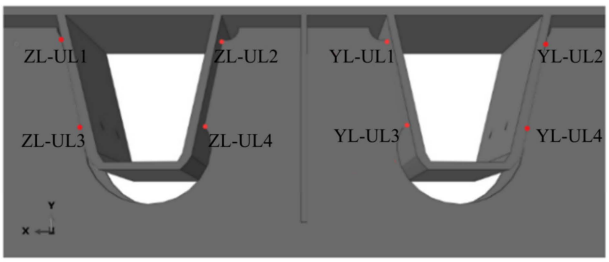

(**c**)

Figure 6. Schematics of strain gauge arrangement: (**a**) strain gauges at bridge decks; (**b**) strain gauges at diaphragms; and (**c**) strain gauges at U-ribs.

2.3. Simulation Scheme of Different Components

After verifying the ABAQUS model, it becomes imperative to optimize the design parameters. While previous studies have provided some basic parameter ranges, the timeliness of these parameters constantly evolves with economic development and changes in vehicle loads. Consequently, to examine the influence of the parameters on the stress of different components, it is necessary to conduct the relevant analyses. The simulation schemes of the specimens with different thicknesses are shown in Table 3.

Table 3. The simulation schemes of specimens with different component thicknesses.

Specimens	Deck Thickness (mm)	U-Rib Thickness (mm)	Diaphragm Thickness (mm)
SJ-DB-14	14	8	14
SJ-DB-16	16	8	14
SJ-DB-18	18	8	14
SJ-DB-20	20	8	14
SJ-HGB-10	16	8	10
SJ-HGB-12	16	8	12
SJ-HGB-14	16	8	14
SJ-HGB-16	16	8	16
SJ-UL-6	16	6	14
SJ-UL-8	16	8	14
SJ-UL-10	16	10	14

3. Results

3.1. Comparison of Simulation and Experimental Results

In practice, the FEM results usually need to be compared with the experiments [36,37]. In this study, the simulated and experimental values of the bridge deck stresses, diaphragm stresses, and U-rib stresses were collected and compared for each loading condition.

Figure 7 shows the simulated stresses at each test point under different loading conditions. Figure 8 shows the experimentally obtained stresses at each test point under different loading conditions. Table 4 exhibits the error between the simulated and experimental values. The results showed that the curves of the simulated results and the experimental results highly overlap with each other. It can be seen that the errors of the samples were all below 10%. The largest errors occurred at test points ZL-DB2 and YL-UL3 under loading condition 2, which might be due to loose strain gauges. On the other hand, the closer the test point is to the loading location, the higher the stress value, which is consistent with the real-world state of stress distribution. Overall, the FEM established in this paper is quite reliable, which could provide a solid foundation for the subsequent optimization of bridge components.

Table 4. Simulation error statistics.

Test Points	Error of Loading Condition 1	Error of Loading Condition 2	Error of Loading Condition 3
ZL-DB1	−3.4%	4.5%	5.5%
ZL-DB2	1.7%	6.7%	3.0%
YL-DB1	−1.7%	−1.8%	−0.5%
YL-DB2	−1.7%	−1.1%	1.8%
ZL-HGB1	1.6%	2.8%	4.2%
ZL-HGB2	0.9%	6.5%	3.9%
YL-HGB1	0.8%	−0.5%	−0.7%
YL-HGB2	−0.3%	−0.7%	−0.4%
ZL-HGB3	1.8%	1.7%	4.7%
ZL-HGB4	0.5%	−1.5%	1.9%
YL-HGB3	0.6%	1.1%	0.4%
YL-HGB4	1.3%	1.1%	−0.1%
ZL-HGB5	0.9%	−1.8%	−3.7%
ZL-HGB6	−0.5%	0.7%	2.8%
YL-HGB5	0.1%	1.7%	−1.8%
YL-HGB6	−0.5%	2.3%	2.4%
ZL-UL1	0.6%	4.0%	5.0%
ZL-UL2	0.7%	3.0%	4.0%
ZL-UL3	−5.0%	5.0%	5.3%
ZL-UL4	2.0%	−5.0%	2.3%
YL-UL1	−0.5%	1.4%	0.5%
YL-UL2	−1.0%	−0.2%	−0.5%
YL-UL3	4.0%	6.7%	4.5%
YL-UL4	6.0%	−4.0%	4.0%

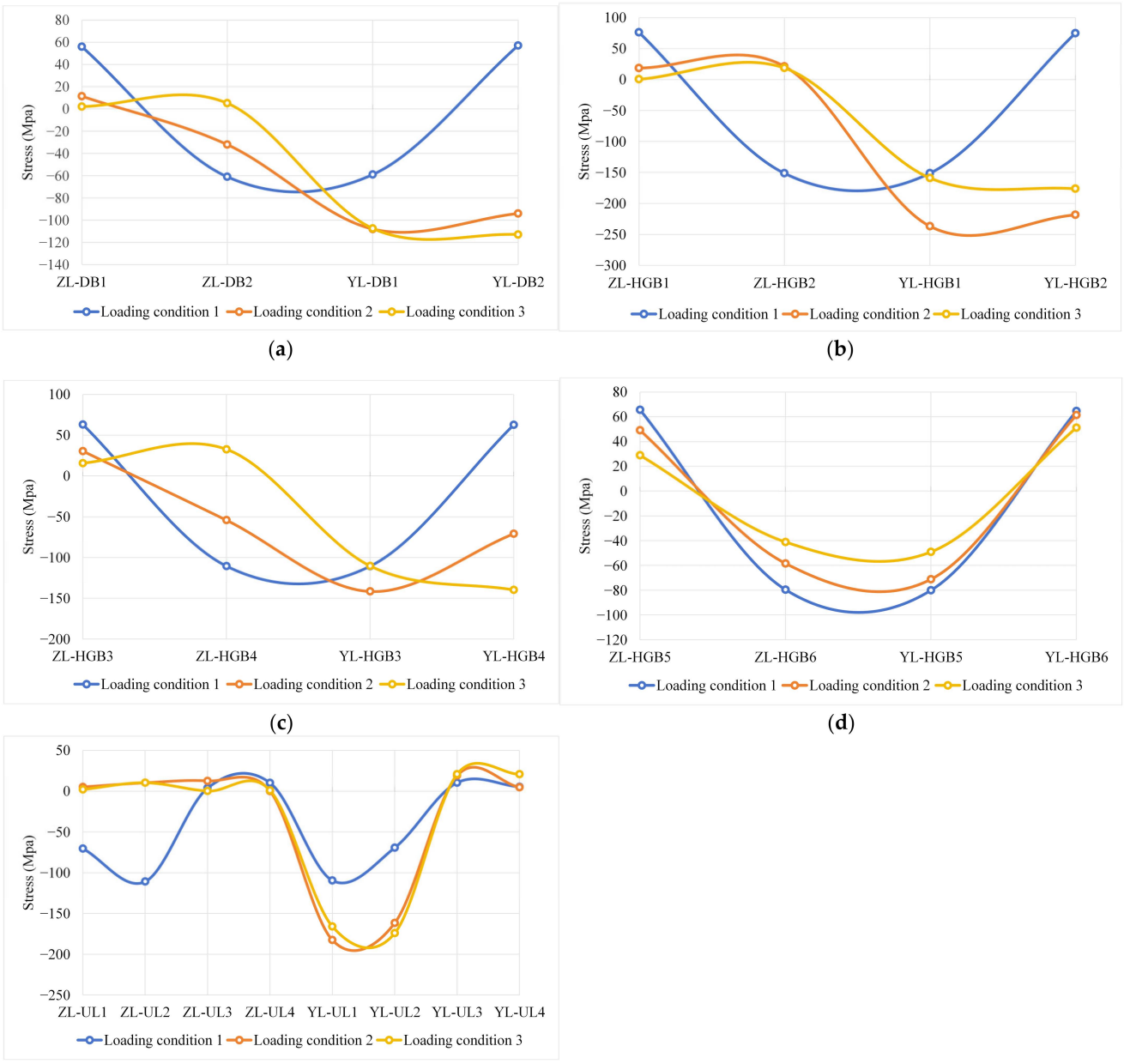

Figure 7. Simulated stresses of different components: (**a**) stresses at the bridge deck; (**b**) stresses at the junction of the diaphragm and bridge deck; (**c**) stresses at the upper opening of the diaphragm; (**d**) stresses at the lower opening of the diaphragm; and (**e**) stresses at the U-rib.

3.2. Exploration of Different Component Parameters

In this study, we explored the design parameters of steel bridges by varying the thicknesses of the bridge decks, diaphragms, and U-ribs, respectively. Taking loading condition 2 as an example, increasing the thickness of any component will decrease the stress at all the test points, which might be due to the fact that increasing the thickness of the components could reduce the moment of inertia of the cross-section [38]. In addition, increasing the thickness of the components also reduced the risk of stress concentrations. The effect of changing the different component thicknesses is as follows.

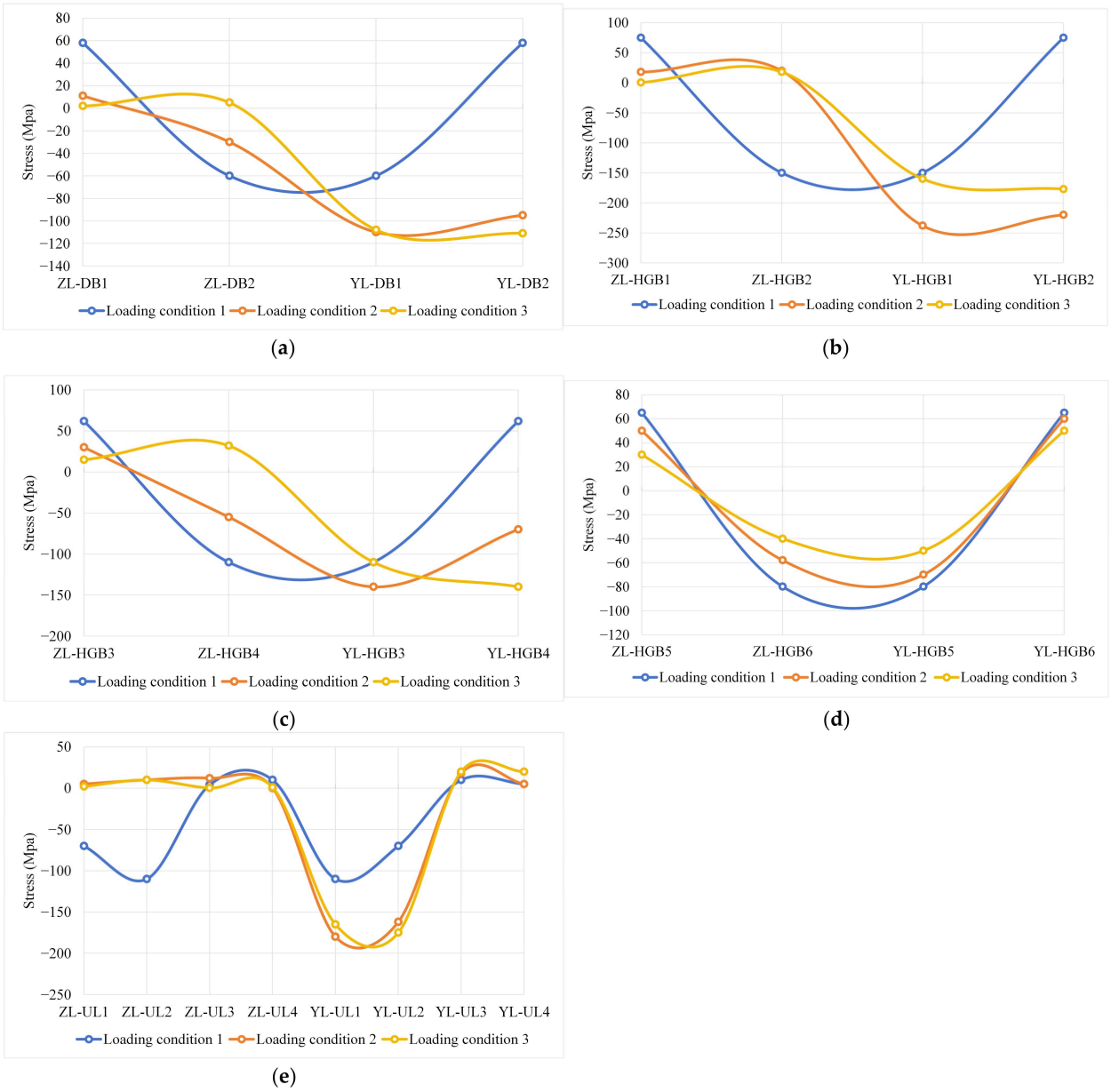

Figure 8. Experimentally obtained stresses of different components: (**a**) stresses at the bridge deck; (**b**) stresses at the junction of the diaphragm and bridge deck; (**c**) stresses at the upper opening of the diaphragm; (**d**) stresses at the lower opening of the diaphragm; and (**e**) stresses at the U-rib.

3.2.1. Influence of Bridge Deck Thickness

The effect of bridge deck thickness on the stress of each component is shown in Figure 9. Table 5 exhibits the values at each test point. The results showed that as the thickness of the bridge deck increases, the bridge deck stress, diaphragm stress, and U-rib stress all decreased to some extent. The maximum stress reduction is observed when the thickness of the bridge deck increased from 16 mm to 18 mm. Meanwhile, the stress reduction decreased when the bridge deck thickness increased from 18 mm to 20 mm. So, the optimal thickness range was determined to be 16 mm to 18 mm.

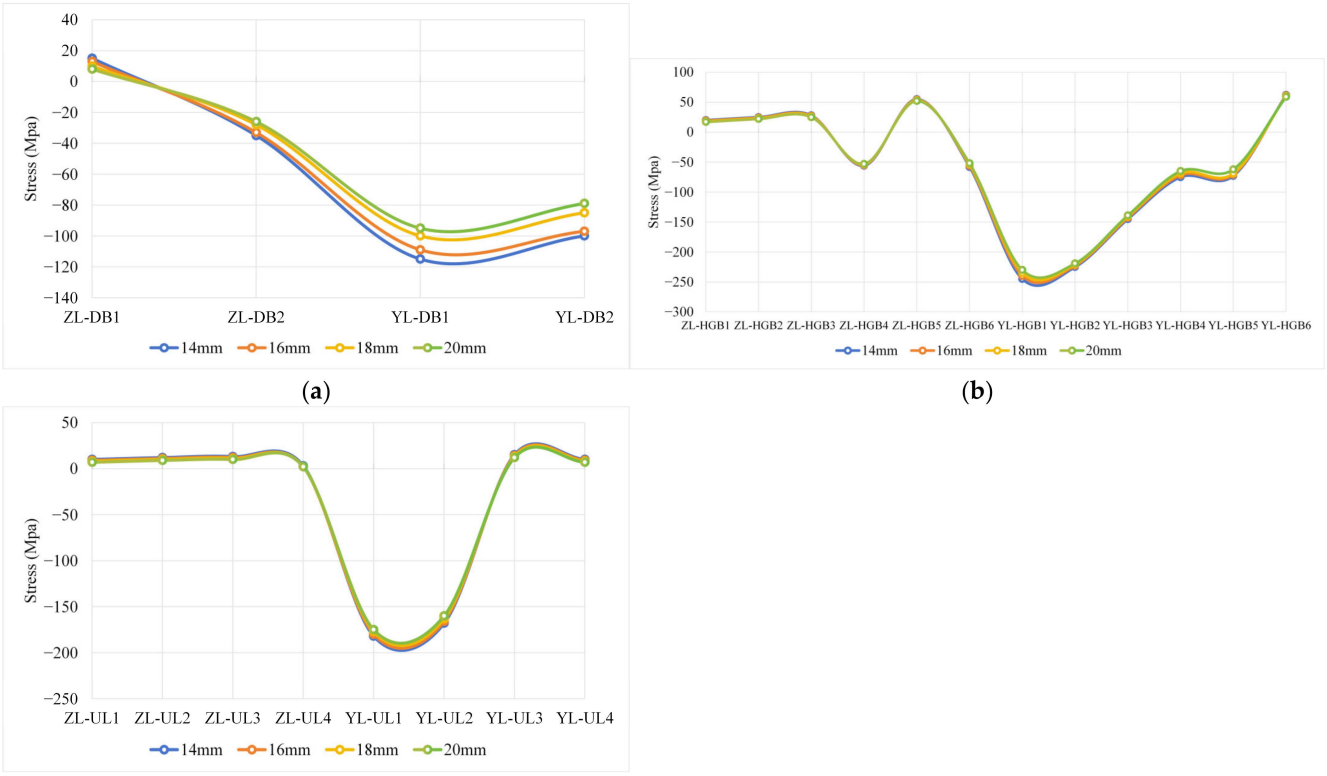

Figure 9. Stress curves under different bridge deck thickness conditions: (**a**) stress curves of bridge deck; (**b**) stress curves of diaphragm; and (**c**) stress curves of U-rib.

Table 5. Stress values at each test point for different bridge deck thicknesses.

Test Points	14 mm (MPa)	16 mm (MPa)	18 mm (MPa)	20 mm (MPa)
ZL-DB1	15	13	10	8
ZL-DB2	−35	−33	−28	−26
YL-DB1	−115	−109	−100	−95
YL-DB2	−100	−97	−85	−79
ZL-HGB1	20	19	18	17
ZL-HGB2	25	24	23	22
ZL-HGB3	28	27	26	25
ZL-HGB4	−56	−55	−54	−53
ZL-HGB5	55	54	53	52
ZL-HGB6	−58	−56	−54	−52
YL-HGB1	−245	−240	−235	−230
YL-HGB2	−225	−223	−221	−219
YL-HGB3	−145	−143	−141	−139
YL-HGB4	−75	−72	−69	−65
YL-HGB5	−73	−71	−69	−62
YL-HGB6	62	61	60	59
ZL-UL1	10	9	8	7
ZL-UL2	12	11	10	9
ZL-UL3	13	12	11	10
ZL-UL4	3	2	2	2
YL-UL1	−182	−180	−177	−175
YL-UL2	−168	−166	−163	−160
YL-UL3	15	14	13	12
YL-UL4	10	9	8	7

3.2.2. Influence of Diaphragm Thickness

The effect of diaphragm thickness on the stress of each component is shown in Figure 10. Table 6 exhibits the values at each test point. The results showed that an increase in the thickness of the diaphragm can also lead to a reduction in the stresses of

the components. The maximum stress reduction was observed when the thickness of the bridge deck increased from 12 mm to 14 mm. Meanwhile, the stress reduction decreased when the diaphragm thickness increased from 14 mm to 16 mm. So, the optimal thickness range was determined to be 12 mm to 14 mm.

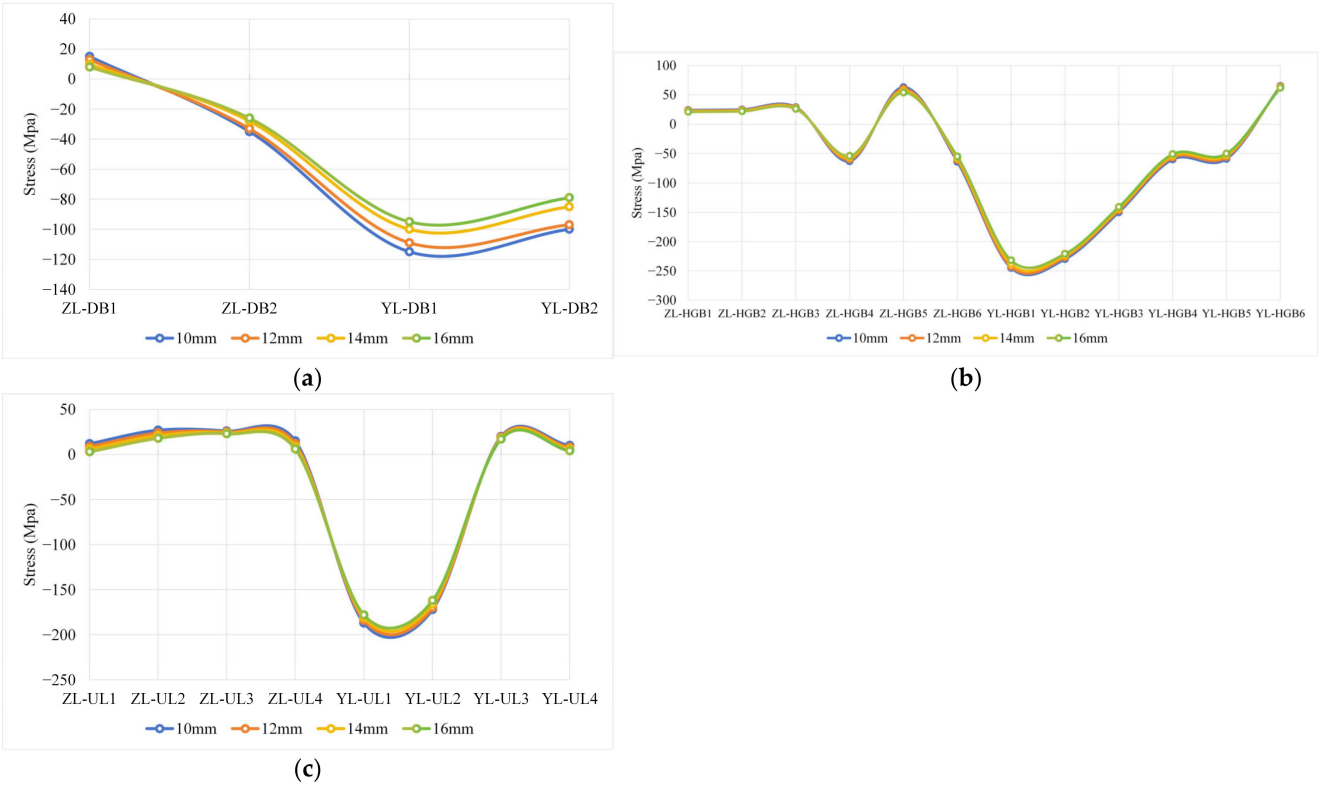

Figure 10. Stress curves under different diaphragm thickness conditions: (**a**) stress curves of bridge deck; (**b**) stress curves of diaphragm; and (**c**) stress curves of U-rib.

Table 6. Stress values at each test point for different diaphragm thickness.

Test Points	10 mm (MPa)	12 mm (MPa)	14 mm (MPa)	16 mm (MPa)
ZL-DB1	15	13	10	8
ZL-DB2	−35	−33	−28	−26
YL-DB1	−115	−109	−100	−95
YL-DB2	−100	−97	−85	−79
ZL-HGB1	24	23	22	21
ZL-HGB2	25	24	23	22
ZL-HGB3	29	28	27	26
ZL-HGB4	−63	−60	−57	−54
ZL-HGB5	63	60	57	54
ZL-HGB6	−64	−61	−58	−55
YL-HGB1	−245	−243	−238	−232
YL-HGB2	−230	−227	−224	−221
YL-HGB3	−150	−147	−144	−141
YL-HGB4	−60	−57	−54	−51
YL-HGB5	−59	−56	−53	−50
YL-HGB6	65	64	63	62
ZL-UL1	12	9	6	3
ZL-UL2	27	24	21	18
ZL-UL3	26	25	24	23
ZL-UL4	15	12	9	6
YL-UL1	−187	−184	−181	−178
YL-UL2	−172	−170	−166	−162
YL-UL3	20	19	18	17
YL-UL4	10	8	6	4

3.2.3. Influence of U-Rib Thickness

The effect of diaphragm thickness on the stress of each component is shown in Figure 11. Table 7 exhibits the values at each test point. The results showed that the thicker the thickness of the U-rib, the lower the stresses of the components. The maximum stress reduction was observed when the thickness of the bridge deck increased from 6 mm to 8 mm. Meanwhile, the stress reduction decreased when the bridge deck thickness increased from 8 mm to 10 mm. So, the optimal thickness range was determined to be 6 mm to 8 mm.

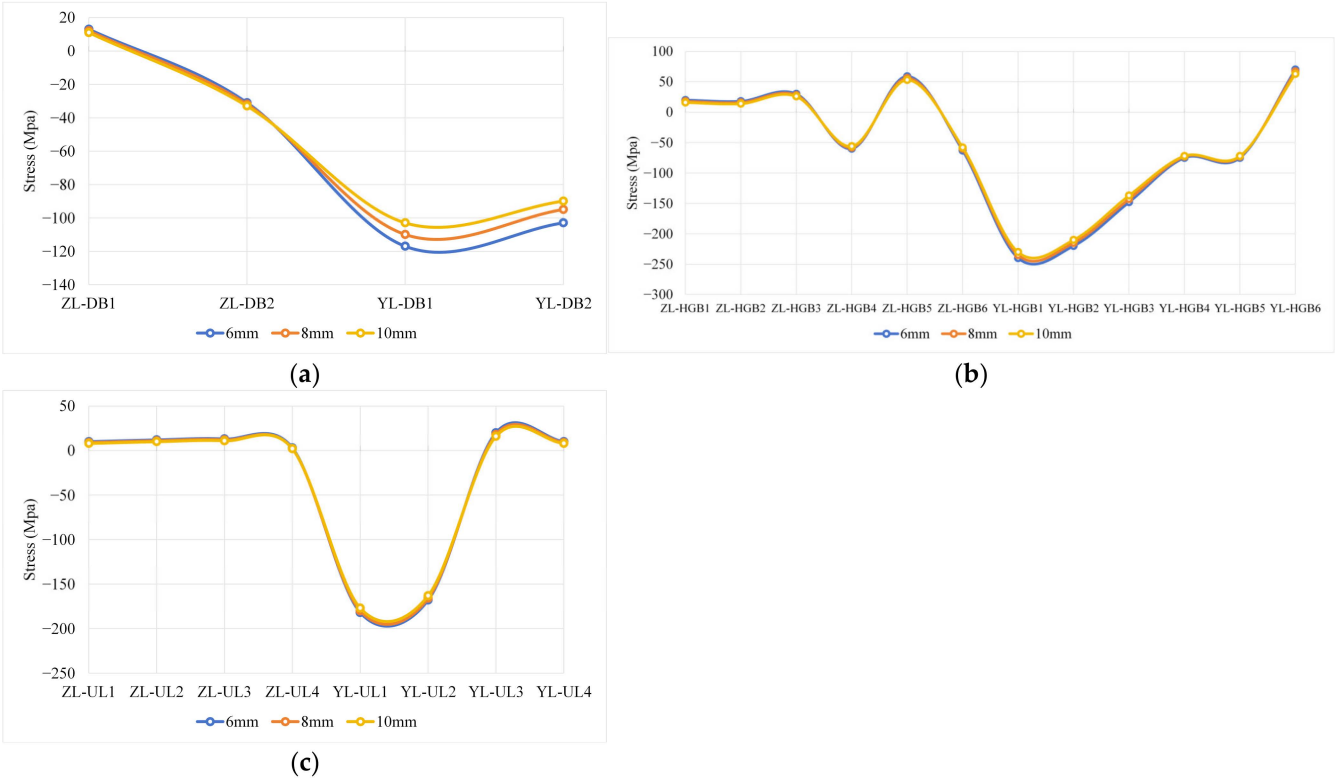

Figure 11. Stress curves under different U-rib thickness conditions: (**a**) stress curves of bridge deck; (**b**) stress curves of diaphragm; and (**c**) stress curves of U-rib.

Table 7. Stress values at each test point for different U-rib thickness.

Test Points	6 mm (MPa)	8 mm (MPa)	10 mm (MPa)
ZL-DB1	13	12	11
ZL-DB2	−31	−32	−33
YL-DB1	−117	−110	−103
YL-DB2	−103	−95	−90
ZL-HGB1	20	18	16
ZL-HGB2	18	16	14
ZL-HGB3	30	28	26
ZL-HGB4	−60	−58	−56
ZL-HGB5	59	56	53
ZL-HGB6	−63	−60	−58
YL-HGB1	−240	−235	−230
YL-HGB2	−220	−215	−210
YL-HGB3	−148	−143	−137
YL-HGB4	−75	−73	−72
YL-HGB5	−75	−73	−72
YL-HGB6	70	67	63
ZL-UL1	10	9	8
ZL-UL2	12	11	10

Table 7. *Cont.*

Test Points	6 mm (MPa)	8 mm (MPa)	10 mm (MPa)
ZL-UL3	13	12	11
ZL-UL4	3	2	2
YL-UL1	−182	−180	−177
YL-UL2	−168	−166	−163
YL-UL3	20	18	16
YL-UL4	10	9	8

4. Discussion

4.1. Application of Experiments and Numerical Simulations in Steel Bridge Design

The steel box girder bridges are subjected to complex loads, which easily result in cracking during use. The optimal design of the bridges is therefore one of the hot topics in recent years. Experiments and numerical simulations are by far the most commonly used methods of addressing this issue [10,11,39,40]. Herzog et al. [41] summarized the study of a large number of model tests and obtained the formula for the stable bearing capacity of steel bridges. Kolstein et al. [42] conducted a study to analyze the stress concentration at steel bridge panel joints by testing with a full-scale steel bridge panel model. Maddox [43] used an FEM to derive the fatigue strength of a steel bridge under repeated vehicle loading. Lin et al. [19] found that encrypted diaphragms can effectively improve the stress performance of steel bridges based on an FEM. On the other hand, the advantages and disadvantages of experiments and numerical simulations are also quite obvious. Generally speaking, an experiment is an effective method to study the stress performance of steel bridges, but in the design of a steel bridge, a large number of experiments are necessary. So, the high costs would limit the application of this method. In contrast, numerical simulations can efficiently and cost-effectively reproduce the stress state of steel bridges under various conditions, but some of the external conditions are usually simplified in the process of numerical modeling. So, the real stress state of steel bridges cannot be completely reproduced. In this study, experiments and numerical simulations were combined to optimize the parameters of a continuous steel box girder bridge, which can save a lot of costs while ensuring accuracy.

4.2. Optimization of Continuous Steel Box Girder Bridge

The optimization of steel bridges needs to ensure good stress performance while considering the economic cost. Ng et al. [44] considered the randomness of vehicle loads in the design of steel bridges and gave a reasonable design range for the dimensions of bridge plates and stiffening ribs. Martins [45] presented an optimized numerical method for the design of bridges, which transformed the design problem of a steel bridge into a multi-objective optimization problem with minimum deflection, minimum stress, and minimum cost. Srinivas et al. [46] investigated an integrated approach for the cost optimization of bridge deck configurations using artificial neural networks (ANNs) and genetic algorithms (GAs), which could significantly reduce the computation costs to find the optimal solution. In this study, the varied thicknesses of bridge decks, diaphragms, and U-ribs were explored based on numerical simulations. A laboratory experiment was carried out to verify the accuracy of the simulation results. Errors below 10% are acceptable when compared to previous studies [32], which set the stage for subsequent studies. The stress analysis results showed that the greater the thickness of the components, the better the stress performance, which might be due to the fact that the increase in component thickness could reduce the moment of inertia of the cross-sections [38]. Considering the stress performance and cost, the optimal ranges of bridge deck thickness, diaphragm thickness, and U-rib thickness were determined to be 18–20 mm, 14–16 mm, and 8–10 mm, respectively.

5. Conclusions

Optimizing the design of steel bridges could ensure their load carrying capacity while reducing construction costs. Previous studies have typically focused on the optimization of a single component. This study explored the optimization of multiple key components, which could provide a more comprehensive optimization scheme. Finally, the optimal range of thicknesses for the bridge decks, diaphragms, and U-ribs were obtained. The following conclusions can be drawn:

(1) The combination of numerical simulations and experiments is an effective method for performing steel bridge design, which can ensure accuracy while reducing costs.
(2) Increasing the thickness of the bridge deck, the thickness of the U-rib, and the thickness of the diaphragm is an effective way to reduce the stresses at each test point.
(3) Considering stress performance and costs, the optimal ranges of bridge deck thickness, diaphragm thickness, and U-rib thickness are determined to be 18–20 mm, 14–16 mm, and 8–10 mm, respectively.

Overall, increasing the thickness of key components is an effective way to optimize steel box bridges. Costs and load-bearing performance need to be considered in a balanced manner. In future studies, More finite element simulations should be carried out to obtain more accurate component thicknesses. In addition, better structural design and material selection need to be further explored.

Author Contributions: Conceptualization, A.W. and R.G.; methodology, Q.C. and W.J.; software, P.F.; validation, A.W., R.G. and W.J.; formal analysis, Q.C.; investigation, R.G.; resources, A.W.; data curation, R.G.; writing—original draft preparation, A.W. and D.W.; writing—review and editing, R.G. and D.W.; visualization, R.G.; supervision, A.W.; project administration, W.J.; funding acquisition, A.W. All authors have read and agreed to the published version of the manuscript.

Funding: This research was funded by the Key Scientific and Technological Projects of Henan Higher Education (Grant No. 23B560015) and Key Scientific and Technological Projects of Henan Province 2022 (Grant No. 222102320267).

Data Availability Statement: The data presented in this study are available upon request from the corresponding author.

Acknowledgments: All authors thank the editors and reviewers for their work on this manuscript.

Conflicts of Interest: The authors declare no conflicts of interest.

References

1. Cheng, Z. Fatigue Life Analysis of Orthotropic Steel Bridge Deck Based on Abaqus and Fe-Safe Platforms. Master's Thesis, Chang'an University, Xi'an, China, 30 March 2021.
2. Wang, C.; Fu, B.N.; Zhang, Q.; Feng, Y.C. Fatigue Test on Full-scale Orthotropic Steel Bridge Deck. *China J. Highw. Transp.* **2013**, *26*, 69–76. [CrossRef]
3. Li, C.; Zou, M.; Li, K.; Han, Y.; Yan, H.; Cai, C. A Study on Post-Flutter Characteristics of a Large-Span Double-Deck Steel Truss Main Girder Suspension Bridge. *Buildings* **2024**, *14*, 3206. [CrossRef]
4. Li, X.; Lin, H.; Zhao, A.-A.; Wang, R.; Feng, Z.; Zhang, S.; Wu, B.; Wu, C.; Xu, X. Experimental study on fatigue performance of double welded orthotropic steel bridge deck. *J. Constr. Steel Res.* **2013**, *34*, 22–26. [CrossRef]
5. Di, J.; Ruan, X.; Zhou, X.; Wang, J.; Peng, X. Fatigue Analysis and Verification of Orthotropic Steel Bridge Decks based on Hot Spot Stress Method. *Struct. Eng.* **2021**, *37*, 10–17. [CrossRef]
6. Zhang, Q.H.; Jin, T.; Li, J.; Bu, Y.Z. Study on Reinforcement for Fatigue Cracking of Rib-to-Diaphragm Welded Joints of Steel Bridge Deck. *J. Southwest Jiaotong Univ.* **2022**, *1*, 92–99. [CrossRef]
7. Zhang, Q.-H.; Cui, C.; Bu, Y.-Z.; Liu, Y.-M.; Ye, H.-W. Fatigue tests and fatigue assessment approaches for rib to-diaphragm in steel orthotropic decks. *J. Constr. Steel Res.* **2015**, *114*, 110–118. [CrossRef]
8. Sun, K.; Jiang, X.; Qiang, X.; Lv, Z.; Fan, C. Equivalent Vehicle Model Based on Traffic Flow of Long-Span Steel Box Girder Bridge. *J. Bridge Eng.* **2023**, *28*, 04023061. [CrossRef]

9. Zhu, J.-H.; Wang, C.; Qi, T.-Y.; Zhou, Z.-S. Vehicle Load Identification on Orthotropic Steel Box Beam Bridge Based on the Strain Response Area. *Appl. Sci.* **2022**, *12*, 12394. [CrossRef]
10. Li, C.-Y.; Wang, C.; Yang, Q.-X.; Qi, T.-Y. Identification of Vehicle Loads on an Orthotropic Deck Steel Box Beam Bridge Based on Optimal Combined Strain Influence Lines. *Appl. Sci.* **2022**, *12*, 9848. [CrossRef]
11. Li, C.; Lu, B.; Wang, C.; Peng, W. Dynamic Performance Assessment of a Novel Hybrid Bridge System with Spread Steel Box Girders. *J. Bridge Eng.* **2022**, *27*, 04021097. [CrossRef]
12. Li, X.; Wan, S.; Zhang, Y.; Zhou, M.; Mo, Y. Beam finite element for thin-walled box girders considering shear lag and shear deformation effects. *Eng. Struct.* **2021**, *233*, 111867. [CrossRef]
13. Bonopera, M.; Chang, K.-C.; Tullini, N. Vibration of prestressed beams: Experimental and finite-element analysis of post–tensioned thin-walled box-girders. *J. Constr. Steel Res.* **2023**, *205*, 107854. [CrossRef]
14. Tsakopoulos, P.A.; Fisher, J.W. Full-scale fatigue tests of steel orthotropic decks for the Williamsburg Bridge. *J. Bridge Eng.* **2003**, *8*, 323–333. [CrossRef]
15. Luo, R.; Qu, Z.F.; Wang, Z.Y.; Zhu, Z.H.; Liu, Z. Fatigue Performance Analysis of Orthotropic PBL Shear Key Bridge Deck with Large Longitudinal Ribs. *J. Railw. Sci. Eng.* **2020**, *17*, 2849–2856. [CrossRef]
16. Zhao, Q.; Guo, Z.; Shen, X.; Briseghella, B. Test study on residual stress distribution of hybrid steel u-rib stiffened plates. *J. Constr. Steel Res.* **2016**, *121*, 261–267. [CrossRef]
17. Luo, R.; Ye, M.; Zhang, Y. Study on Influences of Thickness of Flange of U Rib on Mechanical Behaviors of Orthotropic Monolithic Steel Bridge Deck System. *Adv. Mater. Res.* **2010**, *163–167*, 122–126. [CrossRef]
18. Wang, F.; Lyu, Z.-D.; Zhao, Z.; Chen, Q.-K.; Mei, H.-L. Experimental and numerical study on welding residual stress of U-rib stiffened plates. *J. Constr. Steel Res.* **2020**, *175*, 106362. [CrossRef]
19. Lin, M.S.; Gu, P.; Zhou, C. Stress Analysis of Orthotropic Steel Bridge Deck with Closed Ribs. *J. Shijiazhuang Railw. Univ.* **2010**, *23*, 32–35+40. [CrossRef]
20. Li, X.P.; Zhong, Z.H. Calculating the Bending of Reisner Type Finite Plates with Cracks Using the Edge Load Green's Function Method. *J. Comput. Mech.* **1992**, *9*, 139–147.
21. Wei, D.; Liao, J.; Liu, J.; Gao, Y.; Huang, F. Design and Optimization of the Bi-Directional U-Ribbed Stiffening Plate–Concrete Composite Bridge Deck Structure. *Appl. Sci.* **2023**, *13*, 9340. [CrossRef]
22. Fu, Z.; Ji, B.; Zhang, C.; Wang, Q. Fatigue performance of roof and U-rib weld of orthotropic steel bridge deck with different penetration rates. *J. Bridge Eng.* **2017**, *22*, 04017016. [CrossRef]
23. Zhang, Q.H.; Yuan, D.Y.; Wang, B.Z.; Han, R.L.; Li, J. Fatigue Performance of Innovative Both-side Welded Rib-to-deck Joints. *China J. Highw. Transp.* **2020**, *5*, 79–91. [CrossRef]
24. Saunders, J.; Chen, Y.; Marks, J.A.; Hodgson, I.; Sause, R.; Kozy, B.M. Finite-element fatigue analysis of a new rib-to-floor beam connection for orthotropic steel decks. *J. Bridge Eng.* **2021**, *26*, 1–17. [CrossRef]
25. Jiang, X.; Lyu, Z.L.; Qiang, X.H.; Wang, Y.F. Research on Using Fe-SMA Material to Actively Strengthen FatigueCracks of Arc-Cutouts in Diaphragms. *Bridge Constr.* **2024**, *3*, 54–60. [CrossRef]
26. Duan, L.; Yuan, Y.H.; Wang, C.S.; Eugen, B. Review on research of long lasting UHPFRC composite steel bridge deck. *J. Traffic Transp. Eng.* **2024**, *24*, 68–84. [CrossRef]
27. Jiang, X.; Lv, Z.L.; Qiang, X.H.; Song, S.Y. Fatigue performance improvement of U-rib butt-welded connections of steel bridge decks using externally bonded CFRP strips. *Thin Walled Struct.* **2023**, *191*, 111017. [CrossRef]
28. Freitas, S.; Kolstein, H.; Bijlaard, F. Fatigue assessment of full-scale retrofitted orthotropic bridge decks. *J. Bridge Eng.* **2017**, *22*, 04017092. [CrossRef]
29. Chen, S.; Huang, Y.; Gu, P.; Wang, J.-Y. Experimental study on fatigue performance of UHPC-orthotropic steel composite deck. *Thin Walled Struct.* **2019**, *142*, 1–18. [CrossRef]
30. Da, L.-T.; Zhang, Q.-H.; Yuan, D.-Y.; Ma, Y.; Cui, C. A new orthotropic steel deck system incorporating two novel structural details. *J. Constr. Steel Res.* **2022**, *199*, 107633. [CrossRef]
31. De Corte, W. Parametric study of floorbeam cutouts for orthotropic bridge decks to determine shape factors. *Bridge Struct.* **2009**, *5*, 75–85. [CrossRef]
32. Wang, A.; Gao, R.; Li, H.; Li, J.; Li, K. Analysis of Out-of-Plane Displacements of a Light Steel Keel Fireproof Exterior Wall and Its Connection with the Steel Frame. *Buildings* **2024**, *14*, 1564. [CrossRef]
33. Chhetri, S.; Deb, P. Finite Element Analysis of Geogrid-Incorporated Flexible Pavement with Soft Subgrade. *Appl. Sci.* **2024**, *14*, 5798. [CrossRef]
34. Ashok, D.; Mertens, J.; Bahubalendruni, M.V.A.R. Characterization of penetrate and interpenetrate tessellated cellular lattice structures for energy absorption. *Proc. Inst. Mech. Eng. Part L J. Mater. Des. Appl.* **2022**, *237*, 906–913. [CrossRef]
35. Ashok, D.; Bahubalendruni, M.V.A.R.; Mhaskar, A.; Choudhary, V.; Gunji, B.; Turaka, S. Experimental and numerical investigation on 2.5-dimensional nature-inspired infill structures under out-plane quasi-static loading. *J. Process Mech. Eng.* **2023**, 09544089231197853. [CrossRef]

36. Dara, A.; Bahubalendruni, M.V.A.R.; Johnney Mertens, A.; Balamurali, G. Numerical and experimental investigations of novel nature inspired open lattice cellular structures for enhanced stiffness and specific energy absorption. *Mater. Today Commun.* **2022**, *31*, 103286. [CrossRef]
37. Ashok, D.; Bahubalendruni, M.V.A.R.; Mertens, J.; Gunji, B. A novel nature inspired 3D open lattice structure for specific energy absorption. *Proc. Inst. Mech. Eng. Part E: J. Process. Mech. Eng.* **2022**, *236*, 6. [CrossRef]
38. Ashok, D.; Bahubalendruni, M.V.A.R. Design and Characterization of 2.5D Nature-Inspired Infill Structures under Out-Plane Quasi-Static Loading Condition. *Adv. Mater. Sci. Eng.* **2023**, *2023*, 8918937. [CrossRef]
39. Bayat, E.; Bayat, M.; Hafezzadeh, R. Numerical performance assessment of Tuned Mass Dampers to mitigate traffic-induced vibrations of a steel box-girder bridge. *Struct. Eng. Mech.* **2021**, *78*, 125–134. [CrossRef]
40. Michèle, S.P.; Ronaldo, C.B.; Aluísio, J.R.M. Stress concentration in steel bridge orthotropic decks. *J. Constr. Steel Res.* **2005**, *61*, 1172–1184. [CrossRef]
41. Herzog, M.A.M. Simplified design of unstiffened and stiffened plates. *J. Struct. Eng.* **1987**, *113*, 2111–2124. [CrossRef]
42. Kolstein, M.H.; Wardenier, J.; Cuninghame, J.R.; Beales, C.; Bruls, A.; Poleur, E.; Caramelli, S.; Croce, P.; Carracilli, J.; Jacob, B.; et al. Fatigue strength of welded joints in orthotropic steel deck decks. *Weld. World* **1996**, *38*, 175–194.
43. Maddox, S.J. *Fatigue Behaviours of Trapezoidal Stiffener to Deck Plate Welds in Orthotropic Bridge Decks*; Transport and Road Research Laboratory (TRRL), Structures Department, Bridges Division: Crowthorne, UK, 1974.
44. Ng, S.F.; Kulkarni, G.G. Optimum design of longitudinally stiffened simply supported orthotropic bridge decks. *J. Sound Vib.* **1975**, *40*, 273–284. [CrossRef]
45. Martins, A.M.B.; Simões, L.M.C.; Negrão, J.H.J.O. Optimum design of concrete cable-stayed bridges with prestressed decks. *Int. J. Comput. Meth. En.* **2016**, *17*, 339–349. [CrossRef]
46. Srinivas, V.; Ramanjaneyulu, K. An integrated approach for optimum design of bridge decks using genetic algorithms and artificial neural networks. *Adv. Eng. Softw.* **2006**, *38*, 475–487. [CrossRef]